J Ther Eng, Vol. 11, No. 4, pp. 1075−1093, July, 2025

Journal of Thermal Engineering
Web page info: https://jten.yildiz.edu.tr
DOI: 10.14744/thermal.0000965

Research Article

Thermo-hydrodynamic analysis and exergy destruction minimization in a three- dimensional corrugated channel working with a ferrofluid and an external magnetic field

Abdelaziz BOUMAIZA[1,2,*], Mahfoud KADJA[2], Cherif Ould LAHOUCINE[1], Zakaria KOREI[3]

[1]*Laboratory of Applied Mechanics of New Materials - LMANM, Department of Mechanical Engineering, Faculty of Sciences Technology, University of May 8, 1945 Guelma, 2400, Algeria*

[2]*Renewable Energies and Sustainable Development Laboratory, Department of Mechanical Engineering, University of Mentouri Brothers–Constantine, 25130, Algeria*

[3]*Department of Mechanical Engineering, Faculty of Engineering Construction, Mouloud Mammeri University of Tizi-Ouzou, 15000, Algeria*

ARTICLE INFO

Article history
Received: 30 April 2024
Revised: 18 August 2024
Accepted: 24 September 2024

Keywords:
Heat Transfer; Hydrodynamic Behavior; Magnetic Field; Numerical Modeling; Ferrofluid; Exergy Destruction

ABSTRACT

The ever-increasing consumption of limited energy sources has forced researchers and engineers to produce more efficient energy systems in order to use energy sources effectively. Among the existing energy systems, those which are made of corrugated configurations play an important role in heat transfer enhancement in many engineering applications such as heat exchangers, microchannel heat sinks, solar collectors, etc. This paper analyses the influence of an electromagnetic field on the hydrodynamic and thermodynamic behaviours of Fe_3O_4-water flow in a corrugated channel in order optimize its performance. Such analysis has not been thoroughly investigated by other researchers. Three-dimensional numerical modelling was used to conduct this study. It consisted in solving the governing equations for continuity, momentum, and energy using the finite volume method. The following boundary conditions have been imposed in the study: the non-corrugated parts of the channel are thermally insulated, whereas the top and bottom corrugated surfaces receive a uniform heat flux. An external and uniform magnetic field is applied perpendicular to the flow in the corrugated section. This study examines the effects of the magnetic field strength, the Reynolds number (Re), and the nanofluid volume fraction on the channel's heat transfer performance. The analysis of the results reveals that heat transfer is significantly affected by the magnetic field at low Re numbers (less than 400). The presence of a magnetic field, particularly at B = 300G, prominently features the appearance of eddies at Re = 200 and Re = 400. Entropy generation decreases with increasing magnetic field, which is more evident in the B = 200G and B = 300G cases. The Nusselt number increases by more than 80% with B = 300G at a low Reynolds number (Re = 200). Both the thermal and total exergy destruction decrease as the Reynolds number and magnetic field strengths increase, especially in the cases of Re = 200 and Re = 400 with B = 300G. However, an increase in frictional exergy destruction is observed. The minimum total exergy destruction is achieved at Re = 1200, B = 300 G, and a volume fraction of 2%. The thermal exergy destruction and total exergy destruction in the case of B = 300G decrease by 37% compared to water.

***Corresponding author.**
*E-mail address: azize2520@gmail.com

This paper was recommended for publication in revised form by Editor-in-Chief Ahmet Selim Dalkılıc.

The above findings of the present study therefore lead us to draw the inferences that the use of a magnetic field and a ferrofluid can allow us to manufacture very compact heat exchangers for use in industries where the miniaturization of equipments is compulsory.

Cite this article as: Boumaiza A, Kadja M, Lahoucine CO, Korei Z. Thermo-hydrodynamic analysis and exergy destruction minimization in a three- dimensional corrugated channel working with a ferrofluid and an external magnetic field. J Ther Eng 2025;11(4):1075−1093.

INTRODUCTION

Recent academic research has increasingly focused on innovative methods to increase heat transfer through convection phenomena. Techniques such as the application of a magnetic field, the incorporation of corrugated walls, and the use of nanofluids have been explored. These advancements are recognized for their potential to significantly improve the efficiency of various systems, including solar panels and electronic cooling devices. By optimizing heat transfer processes, these methods contribute to more effective thermal management, leading to enhanced performance, reduced energy consumption, and increased longevity of technological and industrial applications.

Corrugated channels are extensively used in plate heat exchangers which are required in the fields of air-conditioning, chemical reactors, thermal power plants, etc. The presence of corrugations in the geometry of these channels promotes turbulence and increases the surface area, leading to improved thermal performance. Such equipments have been extensively studied in recent years. Varol and Oztop [1] demonstrated that corrugated geometries can enhance heat transfer under free convection in a wavy enclosure filled with a single fluid. Additionally, Ahmed [2] reported that corrugated surfaces enhance the heat resistance of enclosures. According to a study by Nasrin et al. [3], using corrugated surfaces instead of flat surfaces results in an average Nusselt number that is 14.7% greater. The impact of corrugated channels on thermal transfer performance was also explored by Ajeel et al. via both numerical and experimental methods [4,5]. Zhang et al. [6] demonstrated that introducing overall curvature in conventional wavy channels improves heat transfer when the wave amplitudes are set to 0 mm, 0.40 mm, and 0.80 mm. However, as the amplitude increases, the positive effect of the curvature on heat transfer diminishes. Tian et al. [7] reported that channels with varying wave patterns generally outperform those with uniform wave patterns in terms of thermal performance. Liu and Chen performed numerical analyses to examine the impact of waveform channels, porous layer characteristics, cooling-wall subcooling, and inlet air mass fractions on flow and condensation at different inlet velocities. These findings, supported by experimental data, reveal that the vortex distribution and air accumulation play crucial roles in influencing the condensation heat transfer [8].

Sheikholeslami et al. [9] conducted an analysis of a photovoltaic thermal unit integrated with a Thermoelectric Generator (TEG) module and a nanofluid filter. These findings revealed that increasing the velocity of the nanofluid filter significantly enhanced the electrical performance of the system. With the addition of a reflector, the electrical efficiency improved by 37.7%. Sheikholeslami and Khalili [10] introduced a cutting-edge design for a photovoltaic thermal system that features a nanofluid splitter. This trailblazing study is the first worldwide study to assess the spectral behaviour of a system and employ nanofluids to enhance irradiation, ensuring that the bandgap wavelength effectively reaches the silicon layer. Roy et al. [11] conducted a numerical study on laminar flow heat transfer using Al_3O_3/ethylene glycol and Al_3O_3/water nanofluids in a radial flow system. Their research revealed a notable increase in the heat transfer rate. They also reported that the wall shear stress increased with both the concentration of nanoparticles and the Reynolds number. Liang Zhang et al. [12] introduced SiO_2 nanoparticles with a size of 15 nm into water. The results demonstrated that the convective heat transfer coefficient of the nanofluids increased by 36.8% compared with that of pure water at the same Reynolds number. The literature includes numerous numerical studies on nanofluids [13-19]. Sheikholeslami et al. [20] reported that the temperature gradient increases with the volume fraction of Fe_3O_4 and the Rayleigh number. The literature includes numerous numerical studies on Fe_3O_4/water [21-29], which have been employed to increase the heat transfer.

Sheikholeslami [30] discussed an innovative numerical approach demonstrating nanofluid magnetohydrodynamic (MHD) flow through a porous enclosure. Additionally, a numerical approach was investigated to analyse the thermal behavior of alumina nanofluids in a duct. A neural network was employed to estimate the heat transfer rate. Sheikholeslami and Ellahi [31] investigated the presence of a magnetic field in a nanofluid flow within a three-dimensional coordinate system. Their study revealed that the presence of the magnetic field increases the resistive (drag) force and reduces the convection current. Lajvardi et al. investigated forced convection heat transfer using a 5% solid volume concentration of Fe_3O_4/water ferrofluid flowing over a hot tube under a constant magnetic field. Their findings revealed that, in the absence of the magnetic field, the use of Fe_3O_4 nanoparticles as a dispersed phase in water does not improve the convective heat tranfer in the laminar flow regime [32]. Qiang et al. [33] reported that as the magnetic field is strengthened parallel to the temperature

gradient, the thermal conductivity of magnetic nanofluids increases. This phenomenon occurs because particle chains form within magnetic nanofluids along the direction of the temperature gradient. These chains establish a highly efficient, low-resistance pathway for energy transmission when the magnetic field aligns with the gradient. Ghufran et al. [34] investigated the forced convection heat transfer of a Fe_3O_4/water nanofluid in a circular tube under the influence of both constant and alternating magnetic fields. The static magnetic field negatively impacted the convective heat transfer capacity of the magnetic nanofluid, whereas the use of an alternating magnetic field increased the heat transfer rate by up to 27.6%. In their study, Fadaei et al. [35] reported that applying a magnetic field intensifies fluid mixing along the pipe length, consequently increasing the Nusselt number. This enhancement underscores the effectiveness of magnetic fields in augmenting heat transfer characteristics within the fluid. Olayemi et al. [36] reported that ferromagnetic Fe_3O_4 nanofluids demonstrate better thermal conductivity than ferromagnetic Mn-ZnFe_2O_4 nanoparticles do. Petrini et al. showed through numerical simulations that the convective heat transfer rate significantly varies depending on the position and orientation of the magnets. They reported that with an optimal magnet configuration, the average Nusselt number increases by more than 51% compared with that under calm flow conditions [37]. Many other studies exist in the literature on the effects of magnetic fields on flow structure and heat transfer [38-41]. All these studies have been published recently and report heat transfer enhancement when the magnetic field is properly oriented.

The effect of a magnetic field on nanofluid entropy and exergy has also been reported in many recently published works. Sheikholeslami [42] conducted a comprehensive study on the entropy and exergy analysis of nanofluid flow through a porous medium under the influence of the Lorentz force. He incorporated the non-Darcy model to simulate the flow dynamics. The results revealed that the Bejan number decreases as the permeability of the porous medium decreases.Tabarhoseini and Sheikholeslami [43] connected the concepts of entropy generation and thermal analysis by developing a mathematical model to study nanofluid flow within the geometry of an evacuated tube. Similar research [44–48] has been conducted on various multiphysics issues.

One can conclude from the above review that magnetic fields play a crucial role in many scientific and engineering fields, yet, to the best of our knowledge, the impact of a uniform magnetic field on convective heat transfer in a three-dimensional, triangle-shaped, corrugated channel filled with ferrofluid Fe_3O_4-water has not been thoroughly studied. In our research, we chose this specific channel geometry to address this gap and to understand the influence of the magnetic field on the thermodynamic and hydrodynamic behaviours of a ferrofluid. This study therefore explores the effects of variations in magnetic field strength (B), particle volume fraction (ϕ), and Reynolds number (Re) on flow dynamics, pressure, entropy generation, and heat transfer of the ferrofluid Fe_3O_4-water.

PROBLEM DESCRIPTION

Figure 1 schematically illustrates the channel model under examination. The model consists of a three-dimensional channel with a width of 50 mm (L1). It features two heights: a maximum of 16 mm and a minimum of 10 mm. The channel incorporates both a corrugated wall and a flat wall. Each adiabatic flat wall extends 40 mm (L2) before and after the corrugated section, with an axial pitch length (e) of 20 mm. The top and bottom corrugated walls are subjected

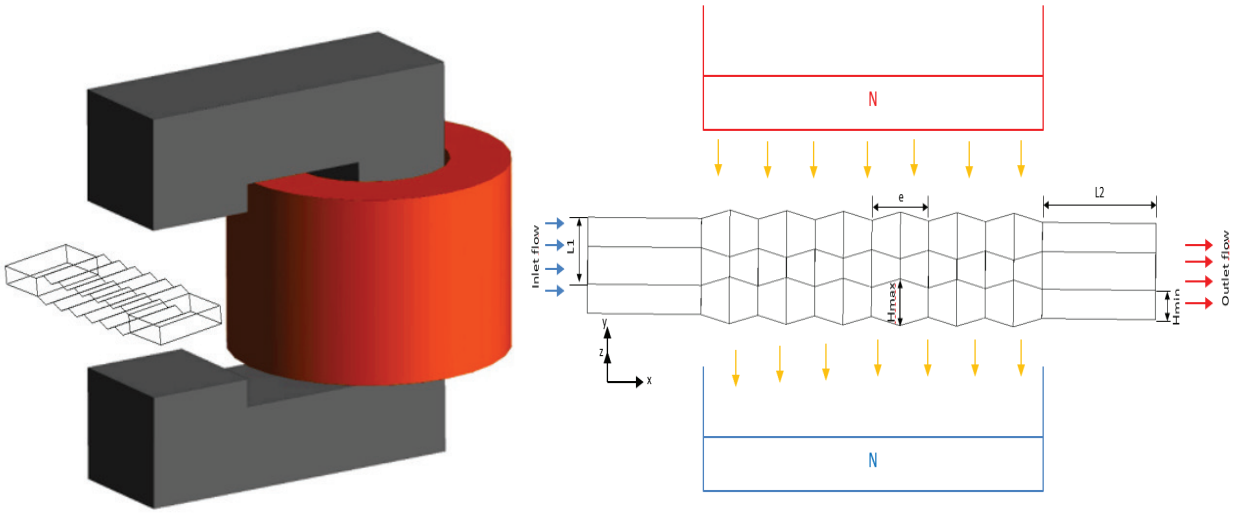

Figure 1. Schematic of the problem studied.

Table 1. Properties of Fe_3O_4 nanoparticles [49]

Material	Diameter (mm)	k (W/m.K)	Cp (J/kg. K)	ρ (kg/ m³)
Fe_3O_4	0.00002	7	640	4950

to a constant heat flux of 50 kW/m², whereas the flat walls are thermally insulated. A uniform magnetic field is applied vertically across the channel. As depicted in Figure 1, this constant magnetic field is generated by an electromagnet. The channel contains an Fe_3O_4-water nanofluid, which is characterized as incompressible and Newtonian. The flow is three-dimensional and laminar. Table 1 provides a summary of the physical characteristics of the magnetite nanoparticles.

The governing equations are derived on the basis of the following assumptions:

- The flow is three-dimensional.
- The ferrofluid behaves as a laminar and incompressible fluid.
- The base fluid and Fe_3O_4 nanoparticles are treated as a single phase.
- The ferrofluid flow follows a Newtonian model.
- The Fe_3O_4 nanoparticles are assumed to be spherical.
- The magnetic field is applied in the Y direction.

The equations are formulated as follows:

Continuity Equation

$$\nabla.\left(\rho_{nf}\,\vec{V}\right)=0 \tag{1}$$

Momentum Equation

$$\nabla.\left(\vec{V}\vec{V}\right)=-\nabla P+\mu_{nf}\nabla^2\,\vec{V}+\overrightarrow{F_k} \tag{2}$$

Energy Equation

$$\nabla.\left(\rho_{nf}C_{p,nf}\,\vec{V}\,T\right)=\nabla.\left(k_{nf}\nabla\mathrm{T}\right) \tag{3}$$

Where $\overrightarrow{F_k}$ is the magnetic volume force, also referred to as the Kelvin body force, and is computed via the following formula:

$$F_K=(\mathrm{M}.\nabla)\,\mathrm{B} \tag{4}$$

Maxwell's equations enable the representation of the magnetic field through equations (5) and (6) [50].

$$\nabla.\vec{\mathrm{H}}=0 \tag{5}$$

$$\nabla.\vec{\mathrm{B}}=0 \tag{6}$$

The following relationship connects M and H:

$$\vec{\mathrm{B}}=\mu_0\left(\vec{\mathrm{M}}+\vec{\mathrm{H}}\right) \tag{7}$$

With the following definition of the magnetization vector [51]:

$$\vec{\mathrm{M}}=\chi_m\vec{\mathrm{H}} \tag{8}$$

The magnetic susceptibility, denoted χ_m, is expressed as follows [51]:

$$\chi_m(\mathrm{T})=\frac{\chi_0}{1+\beta(T-T_0)} \tag{9}$$

Equations 7 and 9 can be used to calculate the magnetic force, as follows [52]:

$$\overrightarrow{F_k}=\frac{1}{2}\mu_0\chi_0(1+\chi_m)\nabla\left(\vec{\mathrm{H}}\times\vec{\mathrm{H}}\right)+\mu_0\chi_m\vec{\mathrm{H}}\left(\left(\vec{\mathrm{H}}.\nabla\right)\chi_m\right) \tag{10}$$

The electrical system is located in the electromagnet air gap, which only has a magnetic field applied in the Y direction [49]. As a consequence, $\overrightarrow{F_k}$ can be expressed in this way:

$$\overrightarrow{F_k}=\mu_0\chi_m H^2\frac{-\chi_0\beta}{[1+\beta(T-T_0)]^2}\frac{\partial T}{\partial y}\vec{j} \tag{11}$$

In the current investigation, the characteristics of pure water were considered to be temperature dependent. Consequently, the models described in reference [53] have been employed:

$$\begin{aligned}\rho_f=&2446-20.674T+0.11576T^2-3.12895\times10^{-4}T^3\\&+4.0505\times10^{-7}T^4-2.0546\times10^{-10}T^5\end{aligned} \tag{12}$$

$$\mu_f=2.414\times10^{-5}\times10^{\left[\frac{247.8}{T-140}\right]} \tag{13}$$

$$k_f=-1.13+9.71\times10^{-3}T-1.31\times10^{-5}T^2 \tag{14}$$

Additionally, the following correlations were found to be appropriate for determining the characteristics of the ferrofluid [54]:

$$\rho_{nf}=(1-\phi)\rho_f+\phi\rho_p \tag{15}$$

$$(\rho c_p)_{nf}=(1-\phi)(\rho c_p)_f+\phi(\rho c_p)_p \tag{16}$$

$$k_{nf}=k_f\left[\frac{(k_{np}+2k_f)-2\phi(k_f-k_{np})}{(k_{np}+2k_f)+\phi(k_f-k_{np})}\right] \tag{17}$$

$$\mu_{nf}=\mu_f(1+2.5\phi)\quad \phi\leqslant2\% \tag{18}$$

Formula for Calculating the Flow Nusselt Number

The definition of the local Nusselt number (Nu_L)is as follows [55]:

$$Nu_L = \frac{h_L D_h}{k_{nf}} \quad (19)$$

where $h_L = \frac{q''}{T_w - T_m}$ is the local heat transfer coefficient.

T_m and T_w stand for the mean temperature of the fluid and the local temperature of the wall, respectively. The average Nusselt number (Nu_{ave}) can be obtained by calculating the average value of the local Nusselt numbers in the top and bottom corrugated walls.

$$Nu_{ave} = \frac{\iint Nu_L dA}{A} \quad (20)$$

Where A is the corrugated walls area.

Formula for Calculating the Entropy Production and Exergy Destruction

The local entropy production is calculated using the following formula [56]:

$$S = S_{ht} + S_{ff} \quad (21)$$

Where S_{ht} and S_{ff} represent the entropy produced by heat transport and fluid friction, respectively.

$$S_{ht} = \frac{k_m}{T_{in}^2}\left[\left(\frac{\partial T}{\partial x}\right)^2 + \left(\frac{\partial T}{\partial y}\right)^2 + \left(\frac{\partial T}{\partial z}\right)^2\right] \quad (22)$$

$$\begin{aligned} S_{ff} = \frac{\mu_m}{T_{in}}\Bigg[2\left(\left(\frac{\partial u_m}{\partial x}\right)^2 + \left(\frac{\partial v_m}{\partial y}\right)^2 + \left(\frac{\partial w_m}{\partial z}\right)^2\right) \\ + \left(\frac{\partial u_m}{\partial y} + \frac{\partial v_m}{\partial x}\right)^2 + \left(\frac{\partial u_m}{\partial z} + \frac{\partial w_m}{\partial x}\right)^2 \\ + \left(\frac{\partial v_m}{\partial z} + \frac{\partial w_m}{\partial y}\right)^2\Bigg] + \frac{\mu_m}{K T_{in}}\left({u_m}^2 + {v_m}^2 + {w_m}^2\right) \end{aligned} \quad (23)$$

The exergy destruction was calculated using the following formula [57]:

$$\text{Exergy destruction} = T_0 S_{gen} \quad (24)$$

Where S_{gen} is the global entropy production and is obtained using the formula:

$$S_{gen} = \iiint S d\mathcal{V} \quad (25)$$

Flow Boundary Conditions

Inlet Conditions

- The ferrofluid enters at a uniform velocity $U_{in,}$ calculated from the Reynolds number using the formula: $\mathrm{Re} = \frac{U_{in} d_h}{\nu}$

  Where d_h is the hydraulic diameter $d_h = \frac{4S_{entry}}{P_{wetted}} = 0.0167$ m S_{entry} being the inlet section and P_{wetted} its wetted perimeter.
- The inlet temperature is uniform and equal to 298 K.

Channel (Boundary) Conditions

- A constant heat flux of 50 kW/m² is applied to the upper and lower corrugated channels.
- The non-corrugated walls are insulated.

Outlet Conditions

- Pressure outlet conditions were applied at the outlet.

Numerical Modelling, Grid Independence, and Numerical Method Validation

The flow and heat transfer governing equations were numerically solved using the ANSYS FLUENT solver, which employs a finite volume approach. User-defined functions (UDFs) were developed and integrated into the program's code to incorporate magnetic effects. The velocity−pressure relationship was managed using a coupled algorithm, which in ANSYS Fluent, simultaneously solves the momentum and continuity equations to ensure accurate and efficient calculation of the interdependent velocity and pressure fields, whereas the convective term was discretized using the second-order upwind method. Residual levels less than 10^{-6} were considered. Six sets of grid systems were evaluated to determine the most suitable mesh that ensures good accuracy. The results, shown in Table 2, depict the Nu variation as a function of the Re for pure water. The various cases did not significantly differ from each other. Therefore, for this study, a grid size of 500,000 was selected. Figure 2 displays the generated grid.

The present results have been validated through two comparisons. The initial validation involved a comparison with earlier research by Ahmed et al. [58], as depicted in Figure 3, which displays the average Nusselt number for

Table 2. The number of elements used for mesh independence

Number of nodes	100,000	200,000	300,000	400,000	500,000	600,000
Re	**Nu**	**Nu**	**Nu**	**Nu**	**Nu**	**Nu**
100	6.51	6.32	6.19	6.16	6.13	6.13
200	8.64	8.25	7.96	7.89	7.82	8.01
400	12.337	11.39	10.65	10.42	10.28	10.22
600	16.083	14.69	13.31	12.95	12.58	12.45
800	19.60	17.99	16.06	15.71	14.92	14.72
1000	22.93	21.199	18.78	18.06	17.31	17.05

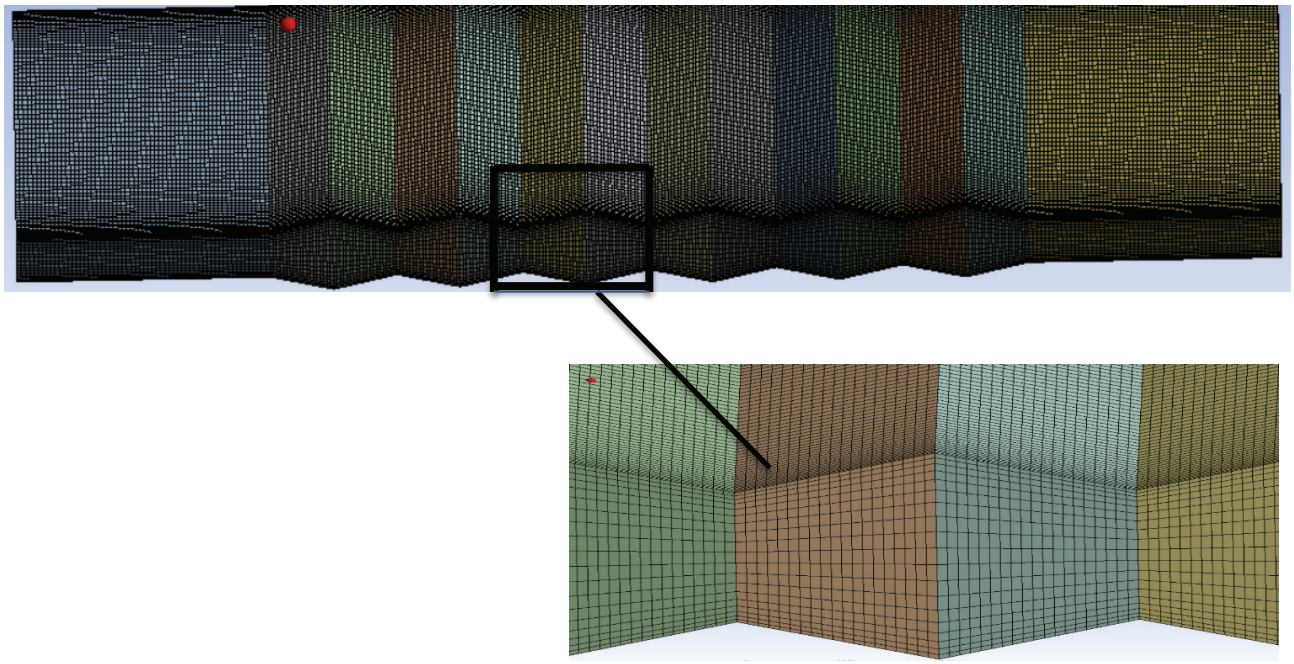

Figure 2. Grid distribution.

pure water at various Reynolds numbers. For the second validation, the experimental data from Ashjaee et al. [59] were used for comparison. Figure 4 compares the local heat transfer coefficient corresponding to a Reynolds number (Re) of 600 at B = 0G and B = 400G.

The comparisons, depicted in Figures 3 and 4, show a strong agreement between the current results and the benchmark values.

RESULTS AND DISCUSSION

In this study, we examine the effect of a magnetic field on the forced convection heat transfer of a ferrofluid in a channel with a corrugated geometry. We present the results by means of the velocity contours, the temperature contours, the entropy contours, the streamlines, the Nusselt number, the pressure drop, and exergy. Additionally, this

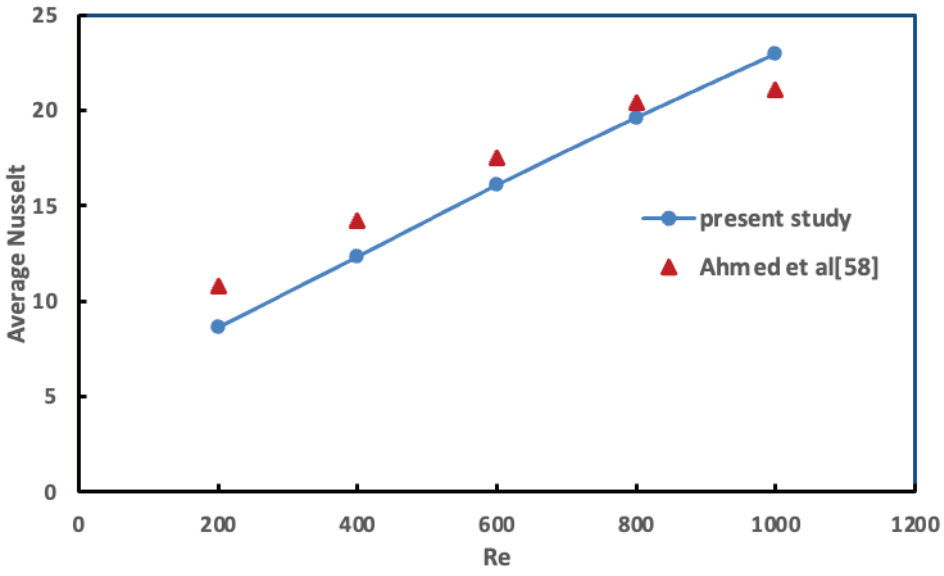

Figure 3. Comparison of the Nu number with the results in the literature.

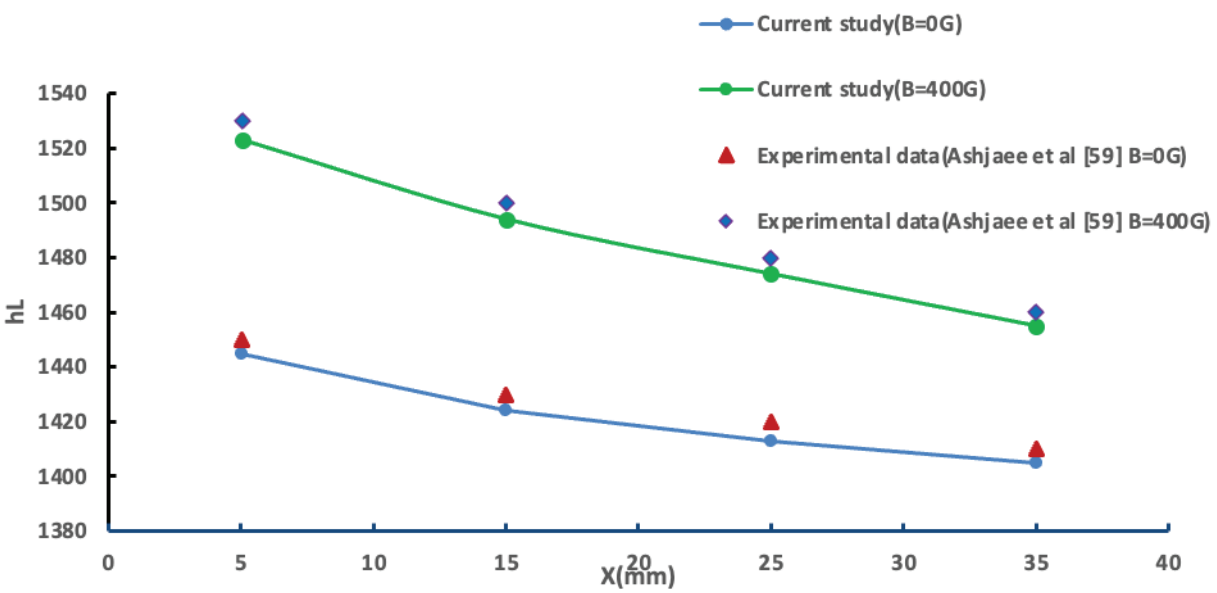

Figure 4. Comparison of the local heat transfer coefficient with the results in the literature.

investigation considers the effects of a 2% volume fraction of nanoparticles and of the Reynolds number Re.

Velocity Contours and Axial Velocity Analysis

Figures 5a-d show the velocity contours in multiple cross-sections along the flow direction and in the symmetry plane at φ = 2% and Re = 200 for B = 0G, B = 100G, B = 200G, and B = 300G; while figure 5e shows the variation of the velocity along the centerline of the symmetry plane for B = 0G and B = 300G. For a given magnetic field and within the entrance region there is formation of the dynamic boundary layer with velocities in the core region becoming more and more greater than those near the channel walls. As soon as the fluid reaches the corrugated region the magnetic force acts in the opposite direction of the flow and therefore the fluid decelerates, it then starts accelerating at the exit of the corrugated region. The boundary layer reaches its quasi-developed state at the outlet of the channel.

Figure 5e clearly shows that for a given magnetic field, the ferrofluid centerline velocity decreases when it crosses the corrugated region. As the magnetic field strength increases, the centerline velocity in the corrugated region decreases. However, in the region preceding the corrugated walls, where there is no magnetic field, the velocity curves coincide with each other.

Temperature Contours and Axial Temperature Analysis

The contours of the temperature along the flow direction and the symmetry plane in various cross-sections at φ = 2% and Re = 200 for the different values of the magnetic field: B = 0G, B = 100G, B = 200G, and B = 300G, are shown in figures 6a-d, while figure 6e shows the variation of the temperature along the centerline of the symmetry plane for B = 0G and B = 300G.

As can be noticed in figures 6a-d, for a given magnetic field and within the entrance region the temperature remains constant. In the corrugated channel the fluid is heated and therefore there is formation of the thermal boundary layer with temperatures in the near wall region becoming more and more greater than those in the core region. As soon as the fluid reaches the exit of the corrugated region the fluid ceases to be heated and therefore conserves the same quasi developed profile throughout the exit flat region of the channel.

As for figure 6e, one can observe that an increase of the magnetic field from 0G to 300G provokes an increase of the transfer of heat by convection and consequently the value of the temperature along the centerline of the symmetry plane increases.

Figures 6a-d also show that for a given Reynolds number, the thermal layer thickening implies an increase in heat transfer and therefore in the temperature gradients near the corrugated wall. This is particularly noticeable in cases B = 200G and B = 300G, where the effect is more significant than in cases B = 0G and B = 100G.

Entropy Contours Analysis

For the different values of the magnetic field: B = 0G, B = 100G, B = 200G, and B = 300G, Figures 7 a-d illustrate the local entropy generation contours at φ = 2% and Re = 200 in various cross-sections along the flow direction and the symmetry plane. Close to the corrugated wall, where the temperature gradients and velocity fluctuations are prominent, entropy generation (Sg) is concentrated. However, entropy creation diminishes when moving towards the channel axis from the corrugated walls because of decreased velocity

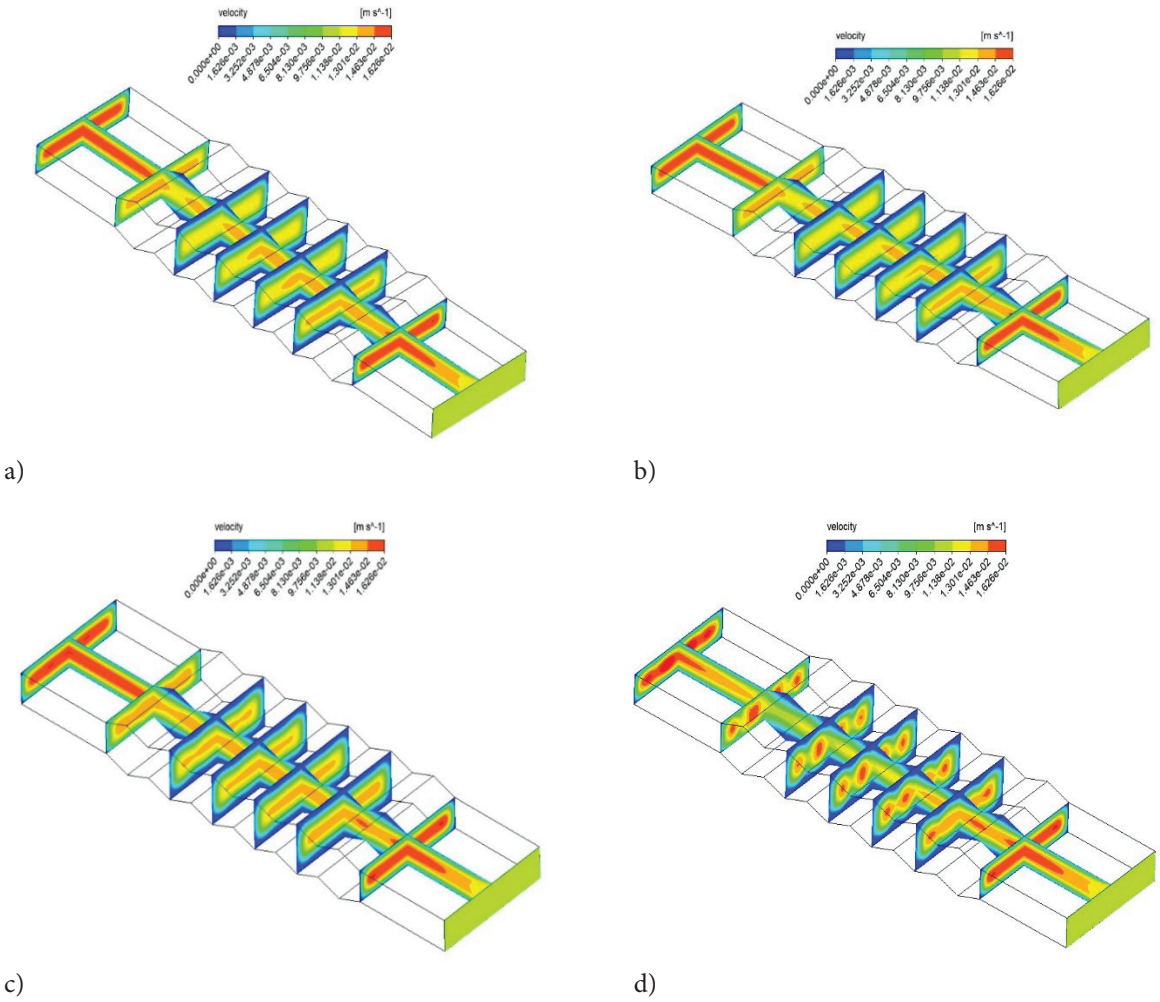

Figure 5a-d. The behaviour of the ferrofluid with and without the magnetic field for φ = 2% and Re = 200 and for the different values of the magnetic field: (a) B = 0G, (b) B = 100G, (c) B = 200G, and (d) B = 300G.

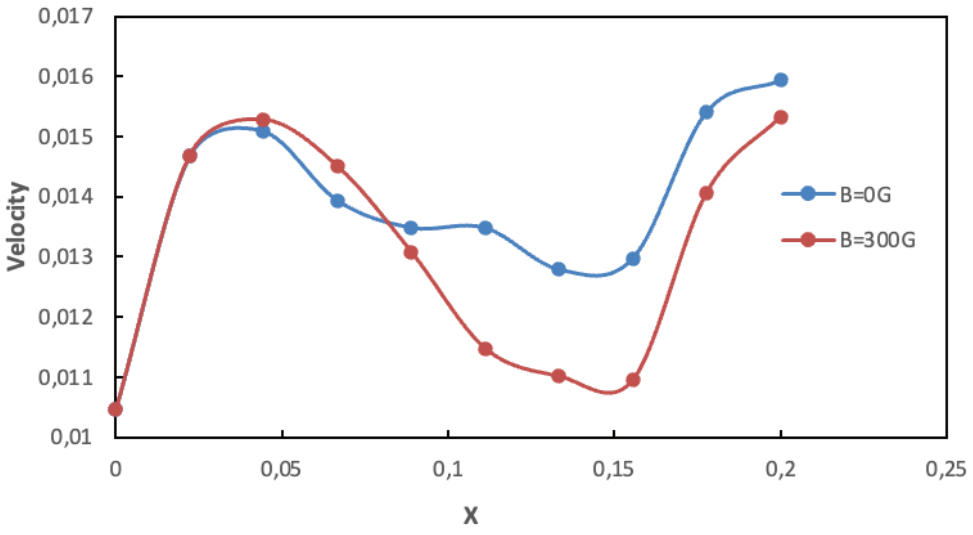

Figure 5e. The velocity distribution along the axis of the channel.

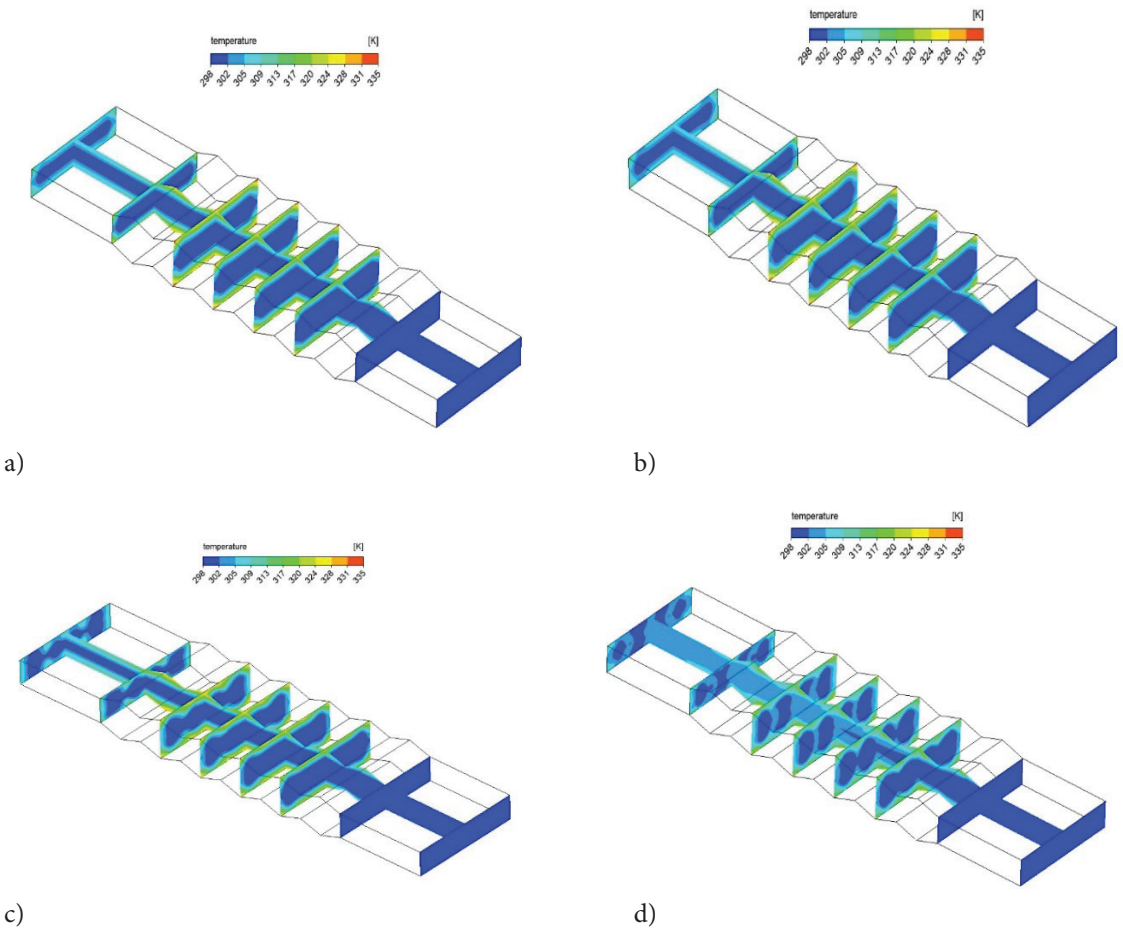

Figure 6 a-d. Temperature contours at φ = 2% and Re = 200 for the different values of the magnetic field: (a) B = 0G, (b) B = 100G, (c) B = 200G, and (d) B = 300G.

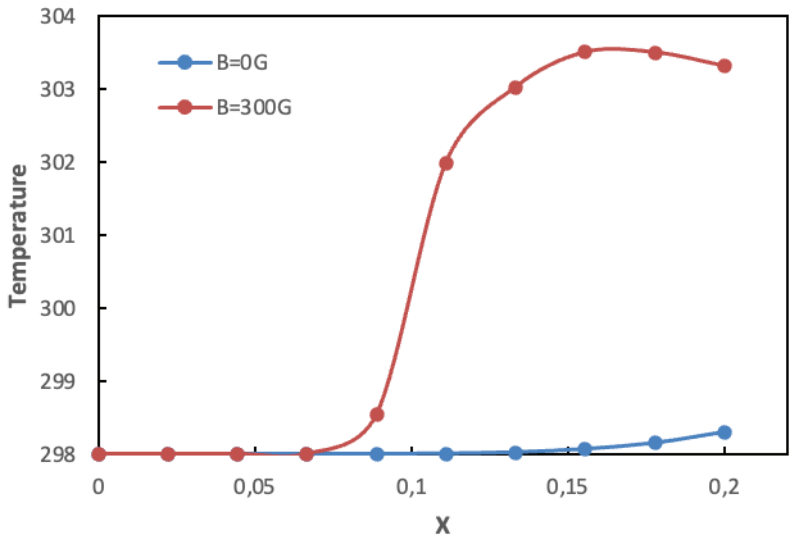

Figure 6e. The temperature distribution along the axis of the channel for Re=200.

and temperature gradients. Furthermore, with an increase in the magnetic field, it appears that entropy generation decreases. This fact is particularly evident in the B = 200G and B = 300G cases, indicating a decrease in energy loss.

Streamlines Contours Analysis

The streamlines comparison in the symmetry plane at φ = 2% for the cases: Re = 200, Re = 400, Re = 600, Re = 900, and Re = 1200, and for B = 0G and B = 300G, is shown in Figures 8 a-e. As can be observed, eddies are more pronounced at higher Reynolds numbers, whether in the presence or absence of a magnetic field. Furthermore, the impact of the magnetic field is more significant at lower Re; eddies at Re = 200 and Re = 400 are clearly visible when a magnetic field is present.

The streamlines for: B = 0G, B = 100G, B = 200G, and B = 300G, are depicted in Figures 9 a-d at φ = 2% and Re = 200. These figures show that an increase in the magnetic field causes more eddies to appear in the corrugated cavities. In the case of B = 300G, the eddies are more noticeable than in the remaining cases.

The streamlines for cases B = 0G, B = 100G, B = 200G, and B = 300G at x = 110 mm, φ = 2%, and Re = 200 are shown in Figures 10 a-d. These figures clearly show that as the magnetic field increases, its influence on the nanofluid becomes more pronounced. The number of eddies increases in the nanofluid; case B = 200G shows a high number of eddies, and case B = 300G shows an even greater number of eddies.

Thermal Analysis

The average Nusselt number for the pure water case (i.e., φ = 0%) and the ferrofluid case (φ = 2%) when B = 0G, B = 100G, B = 200G, and B = 300G are given in Figure 11 and Table 3 for various Reynolds numbers. The figure shows that as Re increases, the average Nusselt number also increases. Furthermore, because Fe_3O_4 has a greater thermal conductivity than pure water, its use leads to a greater value of Nu. Additionally, Nu increases in the corrugated channel due to the presence of the magnetic field, which indicates that the heat transfer is enhanced. In the case of B = 300G, this effect is more noticeable at Re = 200 and Re =

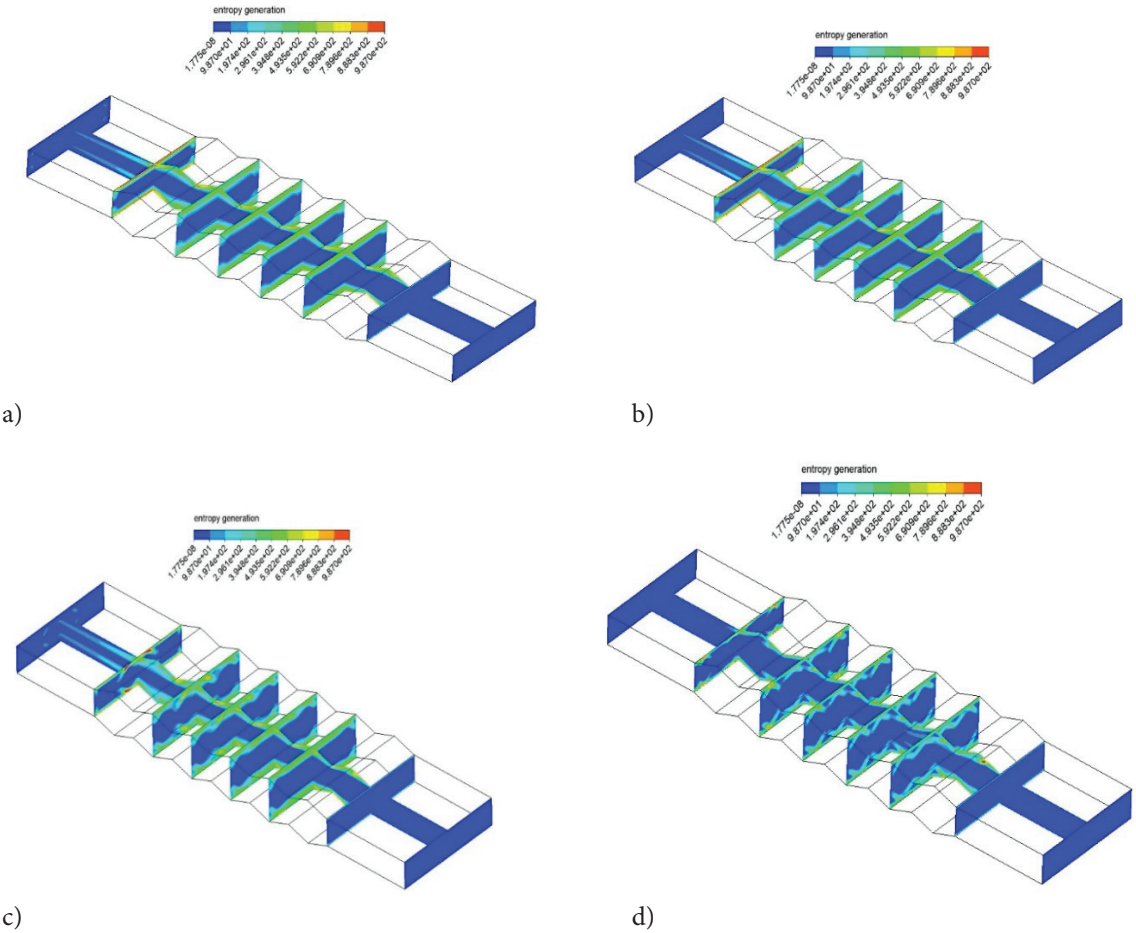

Figure 7 a-d. Local entropy generation contours at φ = 2% and Re = 200 for the cases: (a) B = 0G, (b) B = 100G, (c) B = 200G, and (d) B = 300G.

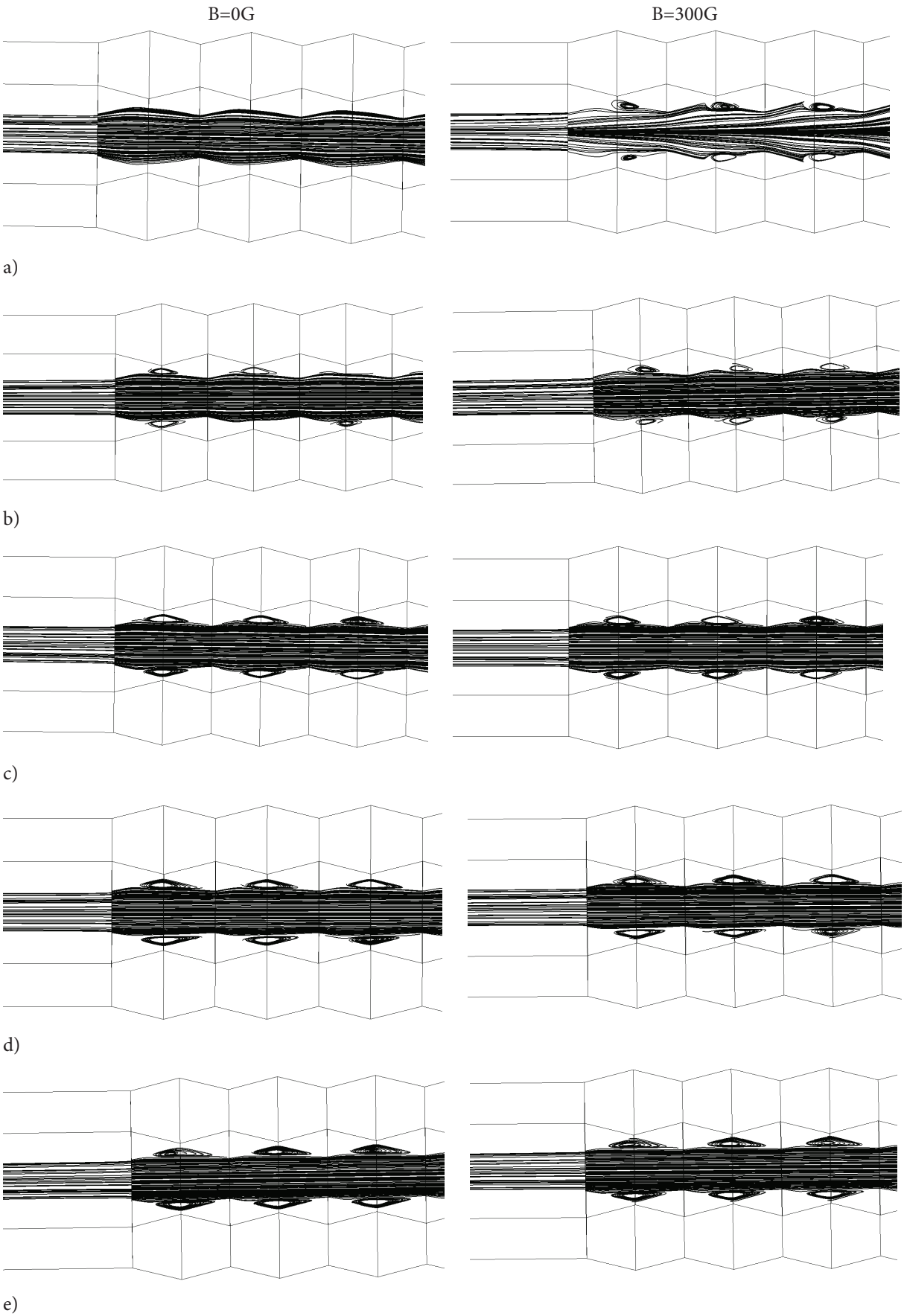

Figure 8 a-e. Streamlines comparison in the symmetry plane at φ= 2% for B = 0G and B = 300G for the cases: (a) Re = 200, (b) Re = 400, (c) Re = 600, (d) Re = 900, and (e) Re = 1200.

400. It follows that at lower Re, the magnetic field appears to have a greater influence on heat transfer. The same behavior of the average Nusselt number (Nu_{ave}) as a function of Reynolds number (Re) and magnetic field was observed by Mehrez and El Cafsi [60] in their study of heat transfer in a horizontal channel. They reported an increase of the

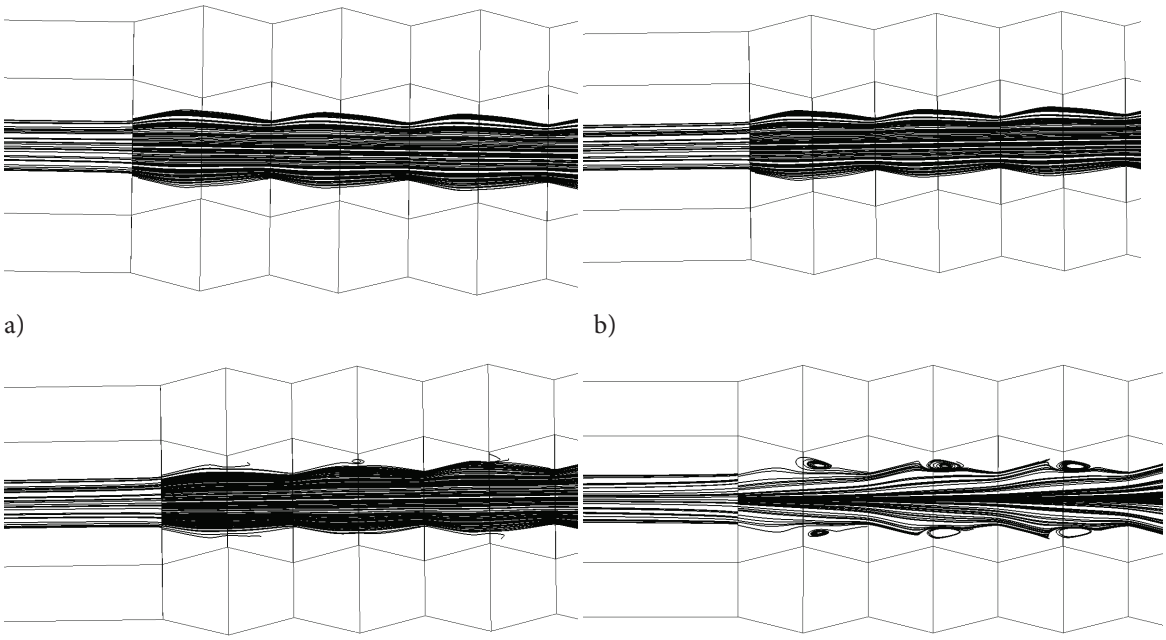

Figure 9 a-d. Streamlines for cases (a) B = 0G, (b) B = 100G, (c) B = 200G, and (d) B = 300G in the symmetry plane at φ = 2% and Re = 200.

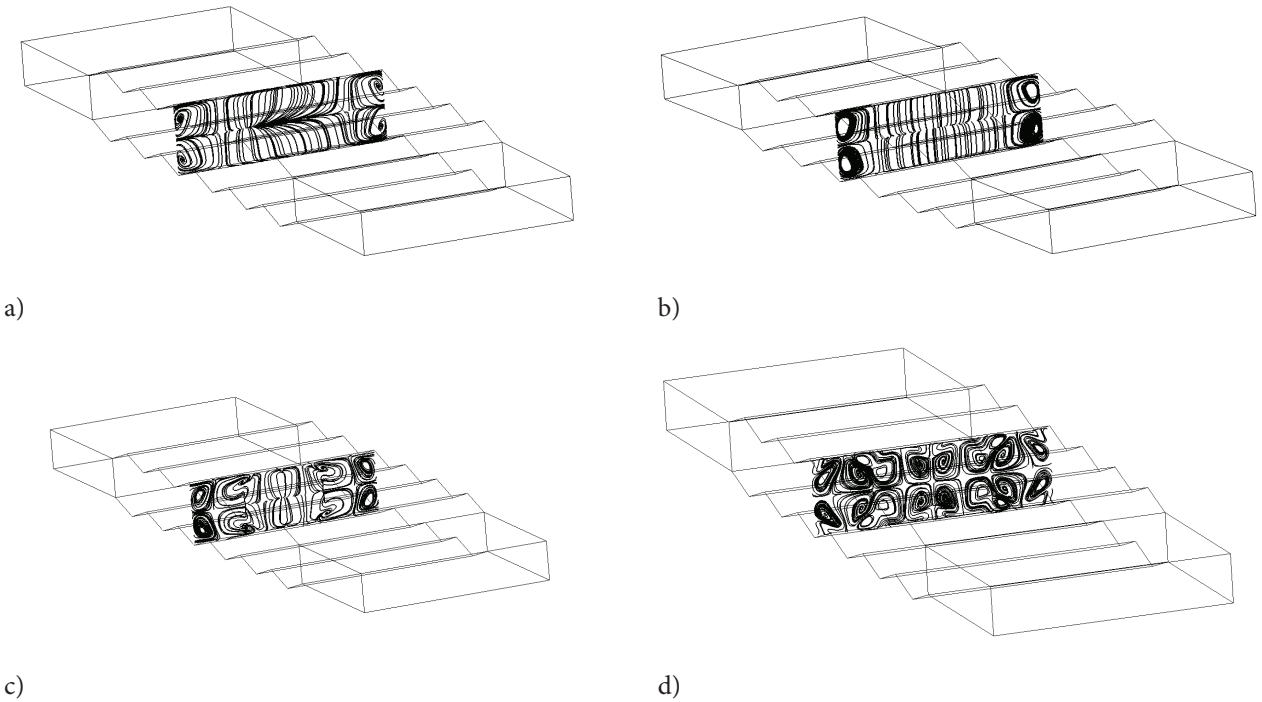

Figure 10 a-d. Streamlines for examples (a) B = 0G, (b) B = 100G, (c) B = 200G, and (d) B = 300G at x = 110 mm, φ = 2%, and Re = 200.

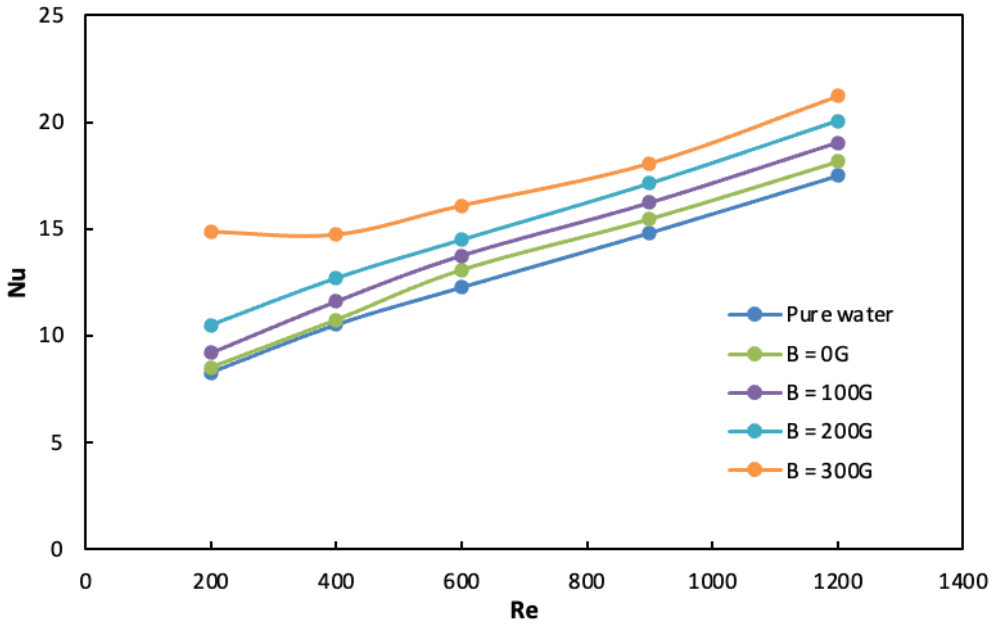

Figure 11. Average Nusselt number for different Re values in the case of pure water (φ = 0%) and ferrofluid (φ = 2%) for B = 0G, B = 100G, B = 200G, and B = 300G.

Table 3. Average Nusselt values

Re	Pure water	B=0G	B=100G	B=200G	B=300G
200	8,268	8,509	9,1877	10,477	14,8417
400	10,509	10,7330	11,5975	12,673	14,71
600	12,263	13,0710	13,742	14,473	16,077
900	14,8232	15,4540	16,217	17,118	18,064
1200	17,5041	18,1380	19,031	20,06	21,229

average Nusselt number as the magnetic field strength or the Reynolds number increase.

Figure 12 and Table 4 show the variations of the average temperature of the corrugated wall under different Reynolds numbers for both the pure water case and the cases B = 0G, B = 100G, B = 200G, and B = 300G at a concentration of φ = 2%. The average temperature in the corrugated wall decreases with increasing Reynolds number when the Fe_3O_4-water nanofluid is used. Additionally, as the magnetic field strength is increased, the temperature further decreased. This explains the rise in Nu in Figure 11, indicating an improvement in heat transfer. The average temperature curves also show that the greatest temperature drops occur when the Reynolds number is increased from Re = 200 to Re = 400.

Hydrodynamic Analysis

Figure 13 shows the pressure drop for various Reynolds numbers in the cases of pure water and B = 0G, B = 100G, B = 200G, and B = 300G at φ = 2%. The pressure drop increases as Re increases. However, the addition of nanoparticles further increased the pressure drop. When a magnetic field is present in the corrugated channel, a slight decrease in the pressure drop is observed as the strength of the magnetic field increases. A similar trend in the evolution of pressure drop (Δp) as a function of the Reynolds number (Re) and the magnetic field was observed by Bezaatpour and Goharkhah [49] in their study on the effects of a uniform external magnetic field and porous fins on convective heat transfer and pressure drop.

Exergy Destruction Analysis

Figures 14-16 show the variation of the thermal exergy destruction, the frictional exergy destruction, and the total exergy destruction with different Reynolds numbers for the cases of pure water and B = 0G, B = 100G, B = 200G, and B = 300G at φ = 2%. These figures illustrate that the exergy destruction decreases as Re increases and when the magnetic field in the corrugated channel increases. Accordingly, the use of a magnetic field reduces energy losses, and its

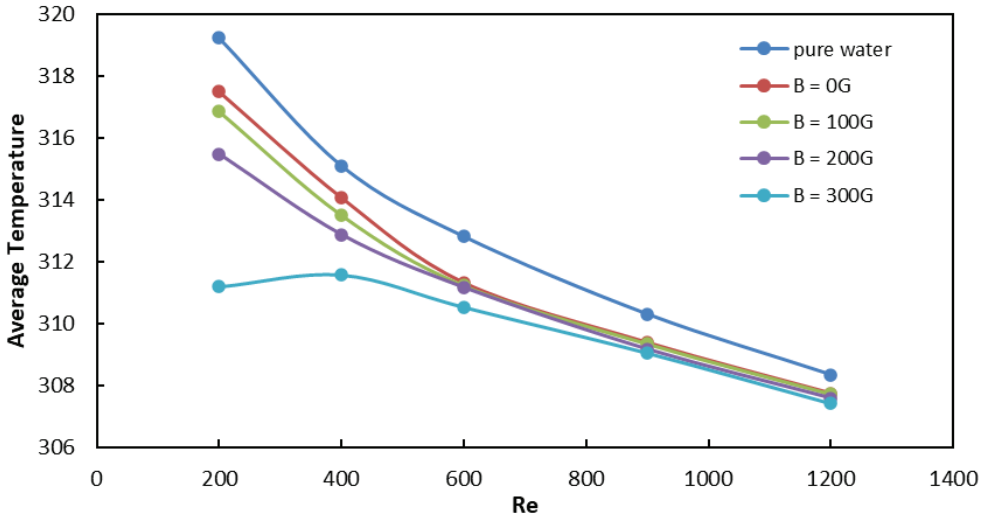

Figure 12. The average temperature in the corrugated wall versus Re for the case of pure water and the cases B = 0G, B = 100G, B = 200G, and B = 300G at φ = 2%.

Table 4. Average Temperature values

Re	Pure water	B=0G	B=100G	B=200G	B=300G
200	319,222	317,495	316,848	315,479	311,194
400	315,097	314,07	313,499	312,878	311,574
600	312,813	311,326	311,229	311,176	310,534
900	310,307	309,391	309,345	309,184	309,052
1200	308,35	307,75	307,722	307,604	307,422

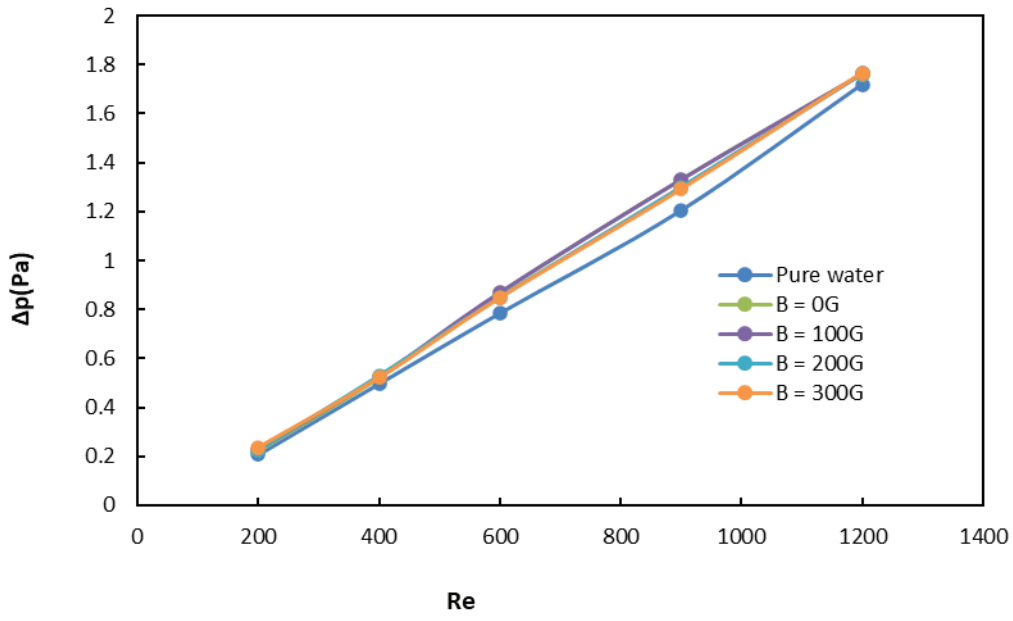

Figure 13. Variation in the pressure drop with Re for the pure water case and the B = 0G, B = 100G, B = 200G, and B = 300G cases at φ = 2%.

effect becomes more noticeable when the Reynolds number is lower than 400. This explains the improved heat transport in the corrugated channel.

Figure 14 shows that the thermal exergy destruction in the corrugated channel decreases as both the Re and magnetic field strengths increase, especially in the cases of Re = 200 and Re = 400 with B = 300G.

According to Figure 15, as Re increases, the value of frictional exergy destruction also increases. In the presence or absence of the magnetic field, the curves are nearly identical.

Since thermal exergy destruction dominates frictional exergy destruction, figure 16 and Table 5 show that the total exergy destruction decreases as Re increases in the presence of a magnetic field. This finding indicates that applying the magnetic field reduces the total energy losses and that the influence of the magnetic field becomes more noticeable at Reynolds numbers lower than 400. This can be considered as a second factor for the enhancement of heat transfer in the corrugated channel besides the high thermal conductivity of the ferrofluid, which is the main factor.

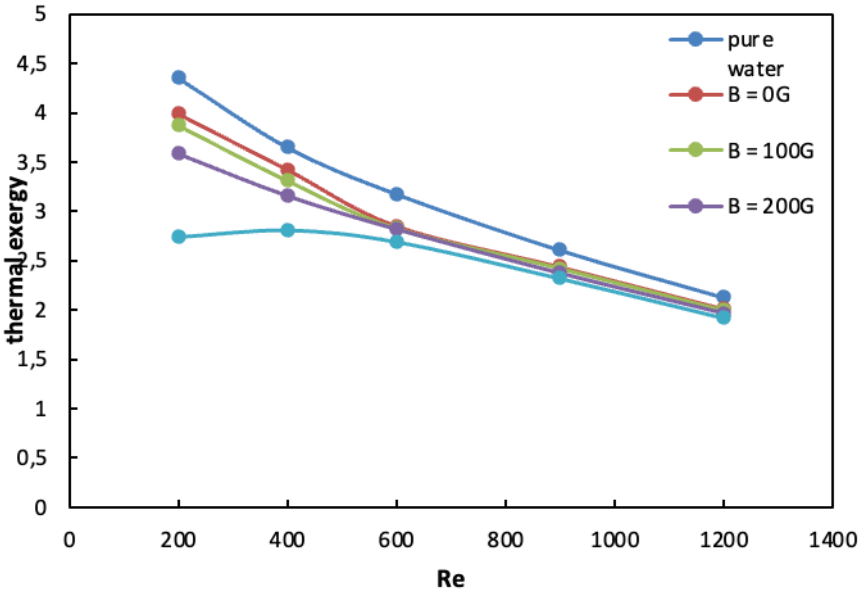

Figure 14. Thermal exergy destruction with Re for the pure water case and the B = 0G, B = 100G, B = 200G, and B = 300G cases at φ = 2%.

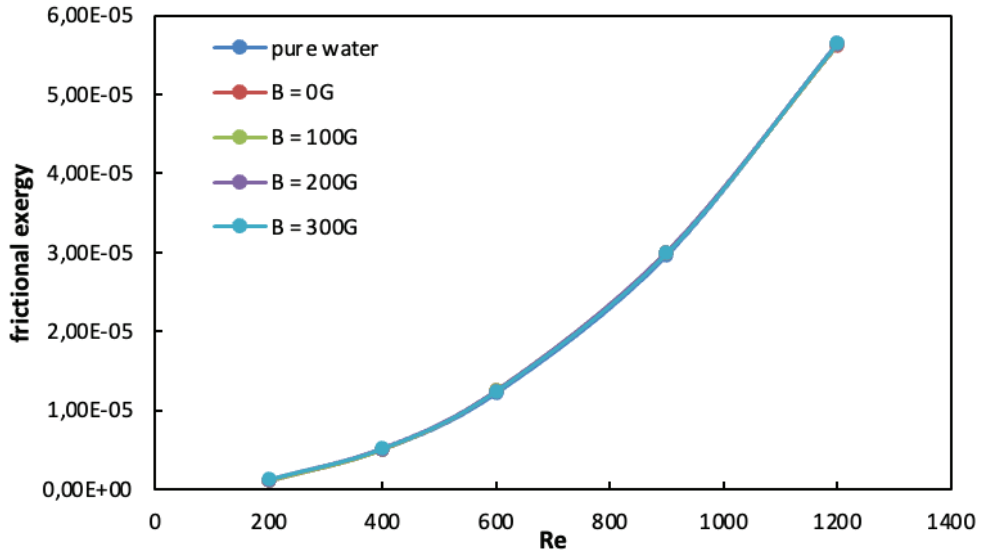

Figure 15. Frictional exergy destruction with Re for the case of pure water and the cases B = 0G, B = 100G, B = 200G, and B = 300G at φ = 2%.

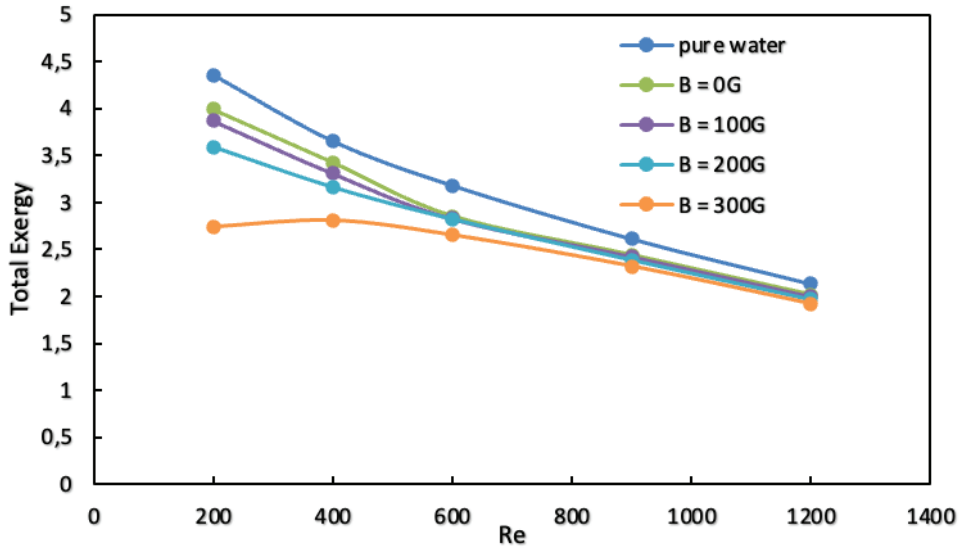

Figure 16. Total exergy destruction with respect to Re for the pure water case and the B = 0G, B = 100G, B = 200G, and B = 300G cases at φ = 2%.

Table 5. Total exergy values

Re	Pure water	B=0G	B=100G	B=200G	B=300G
200	4,3563	3,9909	3,8710	3,5879	2,7419
400	3,6525	3,4259	3,3108	3,1613	2,811
600	3,179	2,854	2,8286	2,8231	2,6543
900	2,61	2,439	2,4254	2,3886	2,3215
1200	2,131	2,014	1,9999	1,9696	1,9202

CONCLUSION

This research presents an in-depth, original numerical investigation of the impact of a uniform magnetic field on ferrofluid flow and heat transfer in triangular corrugated channels. The channel walls at the top and bottom are subjected to a constant heat flux. The numerical findings lead us to several conclusions:

- Owing to the entrainment of ferrofluid in the cavities of the base channel, the magnetic field has a more pronounced effect on heat transfer at Reynolds numbers less than 400.
- Entropy generation decreases with increasing magnetic field, as is more evident in the B = 200G and B = 300G cases.
- When a magnetic field is present, eddies become apparent at Re = 200 and Re = 400, particularly when B = 300G is applied.
- According to our study, at low Reynolds numbers (Re = 200), the Nusselt number increases by more than 80% when B = 300G.
- The corrugated-wall average temperature drop is greater for the low Reynolds number values.
- The pressure drop is not significantly impacted by the magnetic field compared with when it is absent in the triangular corrugated channel.
- The thermal exergy destruction decreases as both the Reynolds number and the magnetic field strengths increase, especially in the cases of Re = 200 and Re = 400 with B = 300G.
- The frictional exergy destruction increases as both the Reynolds number and the magnetic field strength increase.
- The total exergy destruction decreases as both the Reynolds number and the magnetic field strengths increase, especially in the cases of Re = 200 and Re = 400 with B = 300 G, despite an increase in frictional exergy destruction in the triangular corrugated channel.
- The minimum total exergy destruction is achieved at Re = 1200, B = 300G, and φ = 2%.
- The thermal exergy destruction and total exergy destruction in the case of B = 300G decrease by 37% compared to water.

NOMENCLATURE

B	Magnetic flux density (N/A.m)
C_p	Specific heat capacity (J/kg.K)
FM	Body magnetic force (N/ m^3)
H	Intensity of magnetic field (A/m)
h	Local heat transfer coefficient (W/ m^2.K)
k	Thermal conductivity (W/m.K)
M	Magnetization (A/m)
Nu	Average Nusselt number
p	Pressure (Pa)
Re	Reynolds number
S	Entropy (J/K)
T	Average Temperature (K)
x,y,z	Coordinates in Cartesian space (m)
u,v,w	x, y, and z directions' velocities (m/s)

Greek symbols

μ	Dynamic viscosity (kg/m.s)
ρ	Density (kg/ m^3)
φ	Volume fraction of particles
χ_0	Reference magnetic susceptibility
χ_m	Magnetic susceptibility
μ_0	Free space permeability (N/A^2)

Subscripts

f	fluid
n_f	nanofluid
np	nanoparticle

AUTHORSHIP CONTRIBUTIONS

Authors equally contributed to this work.

DATA AVAILABILITY STATEMENT

The authors confirm that the data that supports the findings of this study are available within the article. Raw data that support the finding of this study are available from the corresponding author, upon reasonable request.

CONFLICT OF INTEREST

The author declared no potential conflicts of interest with respect to the research, authorship, and/or publication of this article.

ETHICS

There are no ethical issues with the publication of this manuscript.

STATEMENT ON THE USE OF ARTIFICIAL INTELLIGENCE

Artificial intelligence was not used in the preparation of the article.

REFERENCES

[1] Oztop HF, Varol Y, Koca A. Natural convection in a vertically divided square enclosure by a solid partition into air and water regions. Int J Heat Mass Transf 2009;52:5909−5921. [CrossRef]

[2] Ahmed SE. Effect of fractional derivatives on natural convection in a complex-wavy-wall surrounded enclosure filled with porous media using nanofluids. ZAMM J Appl Math Mech 2020;100:e201800323. [CrossRef]

[3] Nasrin R, Hossain S, Zahan I, Ahmed KFU, Fayaz H. Performance analysis of hybrid/single nanofluids on augmentation of heat transport in lid-driven undulated cavity. Heat Transf 2020;49:4204−4225. [CrossRef]

[4] Ajeel RK, Salim WI. Experimental assessment of heat transfer and pressure drop of nanofluid as a coolant in corrugated channels. J Therm Anal Calorim 2021;144:1161−1173. [CrossRef]

[5] Ajeel RK, Salim WI, Hasnan K. Experimental and numerical investigations of convection heat transfer in corrugated channels using alumina nanofluid under a turbulent flow regime. Chem Eng Res Des 2019;148:202−217. [CrossRef]

[6] Zhang LY, Duan RJ, Che Y, Lu Z, Cui X, Wei LC, et al. A numerical analysis of fluid flow and heat transfer in wavy and curved wavy channels. Int J Therm Sci 2022;171:107248. [CrossRef]

[7] Tian XW, Zhang SZ, Sun C, Wang W. Heat transfer enhancement in cold plates with wavy channels via free-shape modeling and optimization. Int J Therm Sci 2023;193:108446. [CrossRef]

[8] Liu P, Chen W. Thermal-hydraulic characteristics analysis of steam-air condensation in vertical porous-wall corrugated tubes. Appl Therm Eng 2024;236:121688. [CrossRef]

[9] Sheikholeslami M, Khalili Z, Scardi P, Ataollahi N. Environmental and energy assessment of photovoltaic-thermal system combined with a reflector supported by nanofluid filter and a sustainable thermoelectric generator. J Clean Prod 2024;438:140659. [CrossRef]

[10] Sheikholeslami M, Khalili Z. Simulation for impact of nanofluid spectral splitter on efficiency of concentrated solar photovoltaic thermal system. Sustain Cities Soc 2024;101:105139. [CrossRef]

[11] Roy G, Nguyen CT, Lajoie PR. Numerical investigation of laminar flow and heat transfer in a radial flow cooling system with the use of nanofluids. Superlattices Microstruct 2004;35:497−511. [CrossRef]

[12] Zhang L, Zhang A, Jing Y, Qu P, Wu Z. Effect of particle size on the heat transfer performance of SiO_2-water nanofluids. J Phys Chem C 2021;125:13590−13600. [CrossRef]

[13] Esfahani NN, Toghraie D, Afrand M. A new correlation for predicting the thermal conductivity of ZnO–Ag (50%–50%)/water hybrid nanofluid: An experimental study. Powder Technol 2018;323:367–373. [CrossRef]
[14] Afshari A, Akbari M, Toghraie D, Yazdi ME. Experimental investigation of rheological behavior of the hybrid nanofluid of MWCNT–alumina/water (80%)–ethylene-glycol (20%): New correlation and margin of deviation. J Therm Anal Calorim 2018;132:1001–1015. [CrossRef]
[15] Korei Z, Louali K. Prediction of hybrid nanofluids behavior and entropy generation during the cooling of an electronic chip using the Lagrangian–Eulerian approach. Heat Transf 2022;51:6815–6835. [CrossRef]
[16] Akhgar A, Toghraie D. An experimental study on the stability and thermal conductivity of water–ethylene glycol/TiO_2–MWCNTs hybrid nanofluid: Developing a new correlation. Powder Technol 2018;338:806–818. [CrossRef]
[17] Mehrizi AA, Farhadi M, Afroozi HH, Sedighi K, Darz AR. Mixed convection heat transfer in a ventilated cavity with hot obstacle: Effect of nanofluid and outlet port location. Int Commun Heat Mass Transf 2012;39:1000–1008. [CrossRef]
[18] Korei Z, Benissaad S, Filali A, Berrahil F. An investigation of entropy and exergy of nanofluid flow in microchannel heat sinks. J Nanofluids 2023;12:1160–1172. [CrossRef]
[19] Korei Z, Benissaad S, Chamkha AJ, Berrahil F, Filali A. Thermohydraulic and second law analyses during the cooling of an electronic device mounted in an open cavity equipped with magnetic nanofluid, magnetic field inducer, and porous media: A two-phase numerical investigation. Int Commun Heat Mass Transf 2022;139:106497. [CrossRef]
[20] Sheikholeslami M, Ellahi R, Vafai K. Study of Fe_3O_4–water nanofluid with convective heat transfer in the presence of magnetic source. Alex Eng J 2018;57:565–575. [CrossRef]
[21] Fersadou I, Kahalerras H, El Ganaoui M. MHD mixed convection and entropy generation of a nanofluid in a vertical porous channel. Comput Fluids 2015;121:164–179. [CrossRef]
[22] Hussain S, Mehmood K, Sagheer M. MHD mixed convection and entropy generation of water–alumina nanofluid flow in a double lid driven cavity with discrete heating. J Magn Magn Mater 2016;419:140–155. [CrossRef]
[23] Korei Z, Bengherbia N. Heat transfer and thermodynamic analysis of the impact of porous media and nano-powder types in an open cavity equipped with an electronic component. Heat Transf 2022;51:7056–7080. [CrossRef]
[24] Selimefendigil F, Öztop HF. Analysis of MHD mixed convection in a flexible walled and nanofluids filled lid-driven cavity with volumetric heat generation. Int J Mech Sci 2016;118:113–124. [CrossRef]
[25] Job VM, Gunakala SR. Mixed convection nanofluid flows through a grooved channel with internal heat generating solid cylinders in the presence of an applied magnetic field. Int J Heat Mass Transf 2017;107:133–145. [CrossRef]
[26] Haq RU, Hamouch Z, Hussain ST, Mekkaoui T. MHD mixed convection flow along a vertically heated sheet. Int J Hydrogen Energy 2017;42:15925–15932. [CrossRef]
[27] Öztop HF, Sakhrieh A, Abu-Nada E, Al-Salem K. Mixed convection of MHD flow in nanofluid filled and partially heated wavy walled lid-driven enclosure. Int Commun Heat Mass Transf 2017;86:42–51. [CrossRef]
[28] Javed T, Siddiqui MA. Energy transfer through mixed convection within square enclosure containing micropolar fluid with non-uniformly heated bottom wall under the MHD impact. J Mol Liq 2018;249:831–842. [CrossRef]
[29] Maifi T, Sari Hassoun Z, Korei Z, Chamkha AJ. Exploring enhanced heat transfer in wavy porous enclosures: Optimization and analysis of ternary nanofluid integration under varied boundary conditions with MHD mixed convection. Numer Heat Transf A Appl 2024:1–36. [CrossRef]
[30] Sheikholeslami M. Numerical approach for MHD Al_2O_3–water nanofluid transportation inside a permeable medium using innovative computer method. Comput Methods Appl Mech Eng 2019;344:306–318. [CrossRef]
[31] Sheikholeslami M, Ellahi R. Three dimensional mesoscopic simulation of magnetic field effect on natural convection of nanofluid. Int J Heat Mass Transf 2015;89:799–808. [CrossRef]
[32] Lajvardi M, Moghimi-Rad J, Hadi I, Gavili A, Isfahani TD, Zabihi F, et al. Experimental investigation for enhanced ferrofluid heat transfer under magnetic field effect. J Magn Magn Mater 2010;322:3508–3513. [CrossRef]
[33] Li Q, Xuan Y, Wang J. Experimental investigations on transport properties of magnetic fluids. Exp Therm Fluid Sci 2005;30:109–116. [CrossRef]
[34] Ghofrani A, Dibaei MH, Sima AH, Shafii MB. Experimental investigation on laminar forced convection heat transfer of ferrofluids under an alternating magnetic field. Exp Therm Fluid Sci 2013;49:193–200. [CrossRef]
[35] Fadaei F, Shahrokhi M, Dehkordi AM, Abbasi Z. Heat transfer enhancement of Fe_3O_4 ferrofluids in the presence of magnetic field. J Magn Magn Mater 2017;429:314–323. [CrossRef]
[36] Olayemi OA, Obalalu AM, Odetunde CB, Ajala OA. Heat transfer enhancement of magnetized nanofluid flow due to a stretchable rotating disk with variable

thermophysical properties effects. Eur Phys J Plus 2022;137:393. [CrossRef]
[37] Petrini PA, Lester DR, Rosengarten G. Enhanced laminar heat transfer via magnetically driven ferrofluids. Int J Heat Mass Transf 2023;217:124703. [CrossRef]
[38] Varkaneh AS, Nooshabadi GAS, Arani AAA. Flow field and heat transfer of ferromagnetic nanofluid in presence of magnetic field inside a corrugated tube. J Therm Eng 2021;9:1667−1686. [CrossRef]
[39] Rahman H. Investigation of thermomagnetic gravitational convection and energy distribution in a vertical layer of ferrofluid. J Therm Eng 2021;10:936−953. [CrossRef]
[40] Taghikhani MA. Magnetic field effect on the heat transfer in a nanofluid filled lid driven cavity with Joule heating. J Therm Eng 2020;6:521−543. [CrossRef]
[41] Zahmatkesh I. Effect of magnetic field orientation on nanofluid free convection in a porous cavity: A heat visualization study. J Therm Eng 2020;6:170−186. [CrossRef]
[42] Sheikholeslami M. New computational approach for exergy and entropy analysis of nanofluid under the impact of Lorentz force through a porous media. Comput Methods Appl Mech Eng 2019;344:319−333. [CrossRef]
[43] Tabarhoseini SM, Sheikholeslami M. Entropy generation and thermal analysis of nanofluid flow inside the evacuated tube solar collector. Sci Rep 2022;12:1380. [CrossRef]
[44] Sheikholeslami M, Arabkoohsar A, Khan I, Shafee A, Li Z. Impact of Lorentz forces on Fe_3O_4-water ferrofluid entropy and exergy treatment within a permeable semi annulus. J Clean Prod 2019;221:885−898. [CrossRef]
[45] Bhardwaj S, Dalal A, Pati S. Influence of wavy wall and non-uniform heating on natural convection heat transfer and entropy generation inside porous complex enclosure. Energy 2015;79:467−481. [CrossRef]
[46] Chamkha AJ, Selimefendigil F, Oztop HF. MHD mixed convection and entropy generation in a lid-driven triangular cavity for various electrical conductivity models. Entropy 2018;20:903. [CrossRef]
[47] Saboj JH, Nag P, Saha G, Saha SC. Entropy production analysis in an octagonal cavity with an inner cold cylinder: A thermodynamic aspect. Energies 2023;16:5487. [CrossRef]
[48] Saboj JH, Nag P, Saha G, Saha SC. Heat transfer assessment incorporated with entropy generation within a curved corner structure enclosing a cold domain. Heat Transf 2024;53:2460−2479. [CrossRef]
[49] Bezaatpour M, Goharkhah M. Effect of magnetic field on the hydrodynamic and heat transfer of magnetite ferrofluid flow in a porous fin heat sink. J Magn Magn Mater 2019;476:506−515. [CrossRef]
[50] Cheng DK. Fundamentals of engineering electromagnetics. Upper Saddle River (NJ): Pearson; 1993.
[51] Goharkhah M, Bezaatpour M, Javar D. A comparative investigation on the accuracy of magnetic force models in ferrohydrodynamics. Powder Technol 2020;360:1143−1156. [CrossRef]
[52] Hosseinizadeh SE, Majidi S, Goharkhah M, Jahangiri A. Energy and exergy analysis of ferrofluid flow in a triple tube heat exchanger under the influence of an external magnetic field. Therm Sci Eng Prog 2021;25:101019. [CrossRef]
[53] Bergman TL. Fundamentals of heat and mass transfer. Hoboken (NJ): John Wiley & Sons; 2011.
[54] Korei Z, Berrahil F, Filali A, Benissaad S, Boulmerka A. Thermo-magnetic convection analysis of magnetite ferrofluid in an arc-shaped lid-driven electronic chamber with partial heating. J Therm Anal Calorim 2023;148:2585−2604. [CrossRef]
[55] Korei Z, Benissaad S. Turbulent forced convection and entropy analysis of a nanofluid through a 3D 90 elbow using a two-phase approach. Heat Transf 2021;50:8173−8203. [CrossRef]
[56] Bejan A, Tsatsaronis G, Moran MJ. Thermal design and optimization. New York (NY): John Wiley & Sons; 1995.
[57] Ding H, Li Y, Lakzian E, Wen C, Wang C. Entropy generation and exergy destruction in condensing steam flow through turbine blade with surface roughness. Energy Convers Manag 2019;196:1089−1104. [CrossRef]
[58] Ahmed MA, Shuaib NH, Yusoff MZ, Al-Falahi AH. Numerical investigations of flow and heat transfer enhancement in a corrugated channel using nanofluid. Int Commun Heat Mass Transf 2011;38:1368−1375. [CrossRef]
[59] Ashjaee M, Goharkhah M, Khadem LA, Ahmadi R. Effect of magnetic field on the forced convection heat transfer and pressure drop of a magnetic nanofluid in a miniature heat sink. Heat Mass Transf 2015;51:953−964. [CrossRef]
[60] Mehrez Z, El Cafsi A. Heat exchange enhancement of ferrofluid flow into rectangular channel in the presence of a magnetic field. Appl Math Comput 2021;391:125634. [CrossRef]